ACS OMEGA

http://pubs.acs.org/journal/acsodf

Article

Pneumatically Driven Microfluidic Platform and Fully Automated Particle Concentration System for the Capture and Enrichment of Pathogens

Hong Jin Choi, Gna Ahn, U Seok Yu, Eun Jin Kim, Ji-Young Ahn,* and Ok Chan Jeong*

Cite This: *ACS Omega* 2023, 8, 28344−28354

Read Online

ACCESS | Metrics & More | Article Recommendations | Supporting Information

ABSTRACT: In this study, we developed a pneumatically driven microfluidic platform (PDMFP) operated by a fully automated particle concentration system (FAPCS) for the pretreatment of micro- and nano-sized materials. The proposed PDMFP comprises a 3D network with a curved fluidic chamber and channel, five on/off pneumatic valves for blocking fluid flow, and a sieve valve for sequential trapping of microbeads and target particles. Using this setup, concentrated targets are automatically released into an outlet port. The FAPCS mainly comprises solenoid valves, glass reservoirs, a regulator, pressure sensor, main printed circuit board, and liquid crystal display touch panel. All pneumatic valves in the microfluidic platform as well as the working fluids in the glass reservoirs are controlled using FAPCS. The flow rate of the working fluids is measured to demonstrate the sequential programed operation of the proposed pretreatment process using FAPCS. In our study, we successfully achieved rapid and efficient enrichment using PDMFP-FAPCS with fluorescence-labeled *Escherichia coli*. With pretreatment—10 min for the microbead concentration and 25 min for target binding—almost all the target bacteria could be captured. A total of 526 Gram-negative bacteria were attached to 82 beads, whereas Gram-positive bacteria were attached to only 2 of the 100 beads. Finally, we evaluated the PDMFP-FAPCS for SARS-CoV-2 receptor-binding domain (RBD)-based outer membrane vesicles (OMVs) (RBD-OMVs). Specific probes involved in PDMFP-FAPCS successfully isolated RBD-OMVs. Thus, PDMFP-FAPCS exhibits excellent enrichment of particles, including microbes and nanovesicles, and is an effective pretreatment platform for disease diagnosis and investigation.

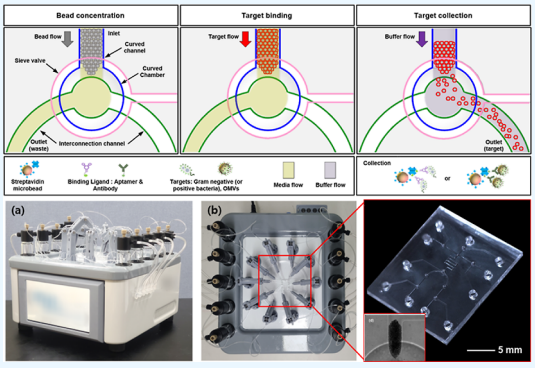

1. INTRODUCTION

Several biomedical studies have focused on analytes attached to fine particles present in samples that contain components of no interest.[1,2] Because the target components exist at moderate or low concentrations in the sample, they must be purified from the original sample or classified according to their properties.[3,4] In certain applications, microparticles functionalized as receptors for specific analytes are used to capture and refine target components.[5,6] Thus, significant research has been conducted on separation and prior concentration using microfluidic technology to reduce the number of steps, number of samples, reagents, and experienced technical staff required.[7]

The latest technologies of lab-on-a-chip have advanced in terms of cost, time, and portability compared to previous technologies, but they lack several key elements for practical application. Larger scale and broader deployment of microfluidic diagnostic systems require automation and integration technologies for (1) cost, (2) improved performance, and (3) portability and simplification.[8−10]

Several microfluidic techniques copy one-to-one techniques found in macro systems; alternatively, micro-phenomena are leveraged to produce the same sample preparation result.[11] Compared to conventional manual processes, sample preparation using microfluidic techniques provides a new path for achieving fast and robust pathogen detection. Microfluidic-based sample preparation methods can be broadly classified into two groups: active and passive.[12,13] Active methods are classified according to the type of external energy applied to the samples, such as magnetophoretic,[14] dielectrophoretic,[15] electrokinetic,[16] and acoustophoretic,[17] which is generally suitable for the precise manipulation of target samples.[18] Passive techniques depend on internal hydrodynamic phenomena such as centrifugal-on-a-chip,[19] sedimentation,[20] hydrodynamic filtration,[21] pinched flow fractionation,[22] lateral displacement,[23] and inertial effects.[24] The advantage of passive technology over active technology is that it is easy to manufacture and operate under high flow rates.[25] In addition, passive techniques may be

Received: April 4, 2023
Accepted: July 14, 2023
Published: July 27, 2023

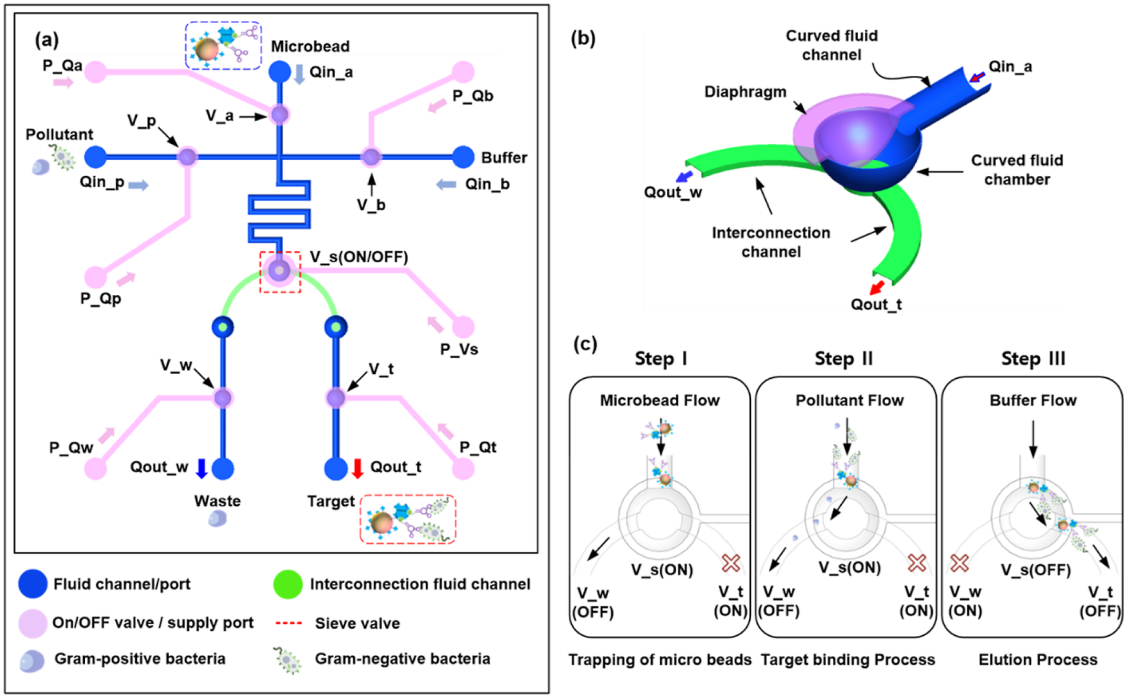

Figure 1. Schematic of PDMFP for concentrating microbead targets (a), structure of the sieve valve to block the microbead (b), and procedure for the pretreatment of the targets [(c), step I to step III]. (P: pneumatic port, in: inlet port, out: outlet port, V: valve, s: sieve, a: antibody-modified bead, b: buffer, w: waste, and t: target.) Three inlet ports exist for specific probe-modified microbeads, target of interests, and buffer. The two outlet ports are for wasting fluid and collecting the target-binding beads.

preferred in applications where energy input is of critical concern.

Owing to the advantages of microfluidic technology, such as high throughput and high content using precise control of small fluid volumes, rapid diagnosis using microfluidic technology is a rapidly growing field, which includes biomedical and clinical diagnoses, food safety, and environmental monitoring.[26−32] However, while microfluidic-based platforms reduce the need for traditional experimental and analytical devices, the operating systems rely on bulky infrastructure such as compression pressure sources, syringe pumps, and desktop computers. Owing to the variety of large-sized operating equipment required for these platforms, critical outdoor applications such as point-of-care diagnosis and environmental monitoring are severely restricted.[33] Thus, an operating system must be developed to commercialize microfluidic technologies.

Recently, a portable automated microfluidic control system using a pump and solenoid valves with microcontrollers was developed to drive a pneumatically driven microfluidic platform (PDMFP).[34,35] It not only reduced the size of the infrastructure and membrane-type elastic microvalves but also successfully demonstrated pressure-driven microfluidics via a host device[33,34] and touchscreen.[35] However, it was not fully integrated, and fluid reservoirs for supplying various fluid samples were not considered. Thus, research on pressure-control systems for both pressure-driven microvalves and fluid flow is necessary.

Advances in nanotechnology-integrated microfluidic systems have the potential to improve biomaterial enrichment.[36] Particularly in the clinical and food industries, the establishment of efficient bacterial pretreatment techniques is crucial for the detection of pathogens. Recently, the detection of extracellular vesicles (EVs) and outer membrane vesicles (OMVs) secreted by bacteria have also become important targets because EVs and OMVs play a role as major transmitters of disease and in host−bacteria interaction.[37,38] Several established methods that rapidly detect microbes in food or clinical samples have enhanced the efficiency of microbial genome extraction.[39] In this study, we evaluated a fully automated particle concentration system (FAPCS) intended specifically for enriching microbes and corona virus receptor-binding domain (RBD)-based OMVs (RBD-OMVs). Gram-negative bacteria, such as *Escherichia coli*, typically cause serious food poisoning, with symptoms such as stomach cramps, diarrhea/bloody diarrhea, and vomiting.[40] Furthermore, in the aftermath of the pandemic, rapid detection of SARS-CoV-2 viruses is essential.[41] To satisfy this requirement, we genetically engineered a viral RBD to harbor the bacterial outer membrane using an antigen 43 autotransporter (AT) system[42] and subsequently purified the nanovesicle OMVs.[43] Herein, we describe proof-of-concept experiments for the enrichment of micro- and nanoparticles. Our PDMFP-FAPCS provides an effective, straightforward, and tunable approach for the preparation of a wide range of biological nano-/microobjects.

2. RESULTS AND DISCUSSION

2.1. Pneumatically Driven Microfluidic Platform.

2.1.1. Structure of PDMFP. Figure 1a shows a schematic of the microfluidic platform used to concentrate a specific target. The proposed microfluidic platform comprises four polydimethylsiloxane (PDMS) layers: an interconnection layer for the pneumatic and fluid supply, a valve diaphragm layer, a 3D fluid network layer with curved fluid channels and valve chambers, and a bottom layer for fluidic sealing without micro structure. The proposed platform has three input ports for introducing specific antibody-modified microbeads (Qin_a), targets (Qin_p), and buffers (Qin_b). Each port is controlled by rubber seal valves (V_a, V_p, and V_b) to prevent reverse leakage of the injected fluid and to control three individual

https://doi.org/10.1021/acsomega.3c02264
ACS Omega 2023, 8, 28344−28354

fluids. When one fluid is injected, the other two completely block the fluid path due to the microvalves. The sieve valve is used to concentrate the antibody-modified microbeads,[44] and the five rubber seal valves are used to block the fluid flow. Two valves (V_w and V_t) are placed at the outlet port. V_w is used to release fluid during the process of concentrating microbeads and binding targets to antibodies attached to microbeads. W_t is used to collect microbeads bound to the target.

2.1.2. PDMFP Pretreatment. Figure 1b illustrates the structure and operational method of the sieve valve for particle concentration. The curved chamber structure was fabricated using the thermal transfer process of an inflated PDMS diaphragm and bonded to the valve diaphragm.[44,45] The valve structure comprises a valve diaphragm, a curved channel and chamber, and an interconnection channel. The antibody-modified microbeads in the working fluid (Qin_a) are blocked by the deformed diaphragm of the sieve valve (V_s) and accumulate in the curved fluid channel. Only the fluid without particles is allowed to flow out via the interconnection channel to the outlet port (Qout_w), whereas the fluid path for the target (Qout_t) is closed using a rubber seal valve (V_t). The antigen can specifically bind to the antibody coated on the surface of the microbeads when the fluid flow for the targets (Qin_p) is introduced. By introducing the buffer and the sequential operation of the pneumatic valves, Qout_w is closed, and antigen-bound microbeads are obtained at the outlet port (Qout_t). Figure 1c shows the two steps of the pretreatment process for specific targets. First, specific antibody-modified microbeads are blocked by the deformed diaphragm of the sieve valve. Subsequently, the specific targets bind the antibody when the target flow is introduced. After two steps, the microbeads bound to the target are eluted at the target port (Qout_t). All processes were programed and performed using FAPCS to detect the target Gram-negative bacteria, *E. coli*, and virus-like outer membrane particles.

2.1.3. Fabrication. Figure 2a shows the fabricated microfluidic platform comprising four PDMS layers: the interconnection layer, the valve diaphragm, layer, the 3D fluid network layer, and the fluid sealing layer. Each layer is fabricated using soft lithography, and their surfaces are modified by corona discharge treatment and sequentially bonded.[46] As shown in Figure 2b, curved structures in the 3D fluid network layer are successfully fabricated using the double-sided replication process of PDMS.[44] The diameter and height of the fluid chamber are 1584 and 188 μm, respectively.

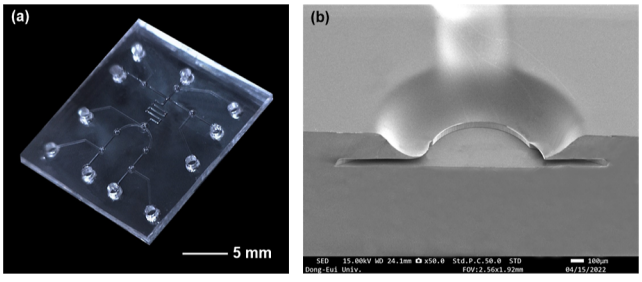

Figure 2. Fabricated PDMFP (a) and the SEM image (b) of the curved fluid chamber and channel structure.

2.1.4. Fully Automated Particle Concentration System. Figure 3a shows a lab-designed FAPCS. The magnitude and frequency of the compressed air is adjusted by varying the current to the solenoid valve to control the flow rate of the target sample, buffer, and bead with the antibody fixed in the reservoir. The fabricated microfluidic platform is mounted on the top of the automation system, and the reserve and inlet ports of the microfluidic platform are connected using a tube. To prevent the tube from escaping owing to pneumatic pressure and flow generation, it is fixed using an arm structure, as shown in Figure 3b,c. The glass reservoir has two tubes: one for pneumatic application and one for fluid transmission. When pneumatic pressure is applied to the properly filled reservoir, the stored fluid is transferred to the microfluidic platform through the fluid tube (Figure S2).

2.1.5. Flow Rate. Figure 4 shows the measured flow rate of the working fluid to demonstrate that the fluid flow is controlled by the programed operation of the microvalves in the microfluidic platform. Table 1 shows the programed sequential signals applied to the pressure control system to operate the microfluidic platform. The flow rate at the two outlet ports is measured with liquid flow sensors (SLI-2000, Sensirion) at a sampling frequency of 12.5 Hz. The pressures on the glass bottles for microbeads, targets, and buffers to generate the flow of fluid are 40, 20, and 70 kPa, respectively. The pressure for the flow of targets and buffers is set to improve the binding efficiency and rapid elution of the target-binding microbeads. If the pressure for the generation of the target flow is too high or too low, the solution containing the targets passes through the concentrated microbeads, which either have limited binding efficiency or block the microchannel. The sieve valve sets the pressure to 80 kPa for a microbead concentration of 10 μm. A pressure of 100 kPa is applied to the microvalves (V_a, V_p, V_b, V_t, and V_w) to block fluid flow. According to a previous work,[44] all particles with three different diameters (4.16, 8.49, and 24.9 μm) were successfully blocked, accumulated, and released. The operating pressure, time required for concentration, and the concentration ratio were dependent on the particle diameter. However, there are three disadvantages in the usage of the small-sized beads (4.16 μm). First, the concentration time of the target sample becomes longer since the hydraulic resistance increases with the increment of the trapped and accumulated particles in the curved microchannel. Second, the unwanted bead aggregation phenomenon frequently occurs during the bead concentration process (step I to II). Thus, the uncertainty in step III for conjugation increases. In addition, it is very hard to collect all beads trapped in the microchannel due to the sticking problem[47−49] on the surface of PDMS. Therefore, based on the experimental experience,[44] beads of the size of 10 μm were properly selected and used for the concentration of bacteria and OMVs.

The flow rate of microbeads introduced into the microfluidic platform in step I was reduced by the sieve valve (Vs) in step II because the fluidic resistance of the microchannel increased as the valve diaphragm deforms when trapping the microbeads. Furthermore, the flow rates (Qin_s) at the outlet ports, Qout_t and Qout_w, were found to be identical. For the target-binding process from the fluid in step III, V_p and V_w were open for the flowing fluid, and V_a, V_b, and V_s were closed to block fluid flow. Thus, Qout_t became zero because of the operation of the pneumatically driven rubber seal valve while a steady flow was observed at the outlet port, Qout_w.[44,45] In step IV, only V_b and V_t were opened to collect the target-binding microbeads, while the other valves were closed. Overall, we measured the flow rate of the working fluid in the microfluidic platform controlled by the on/off rubber seal valves for blocking fluid flow and a sieve valve for sequential trapping of microbeads

https://doi.org/10.1021/acsomega.3c02264
ACS Omega 2023, 8, 28344−28354

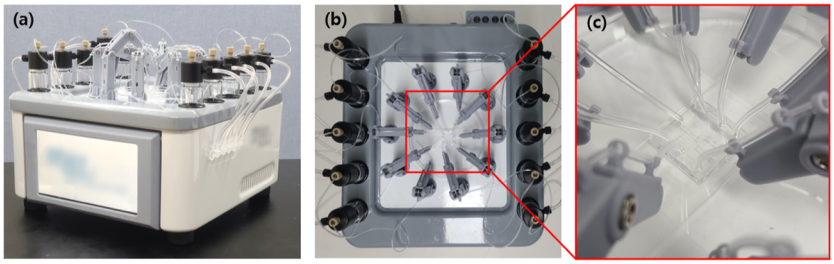

Figure 3. Lab-designed FAPCS (a), its top view (b), and its enlarged view (c). It includes five solenoid valves (ITV0010-3BL) for fluid transfer into the microfluidic platform, five on/off valves (BP-290) for pneumatic valve control inside the microfluidic platform, a regulator for pressure control (ARM10 F2-20BG), a pressure sensor (PSE530), the main printed circuit board for system operation, and a liquid crystal display touch panel for the signal input for control.

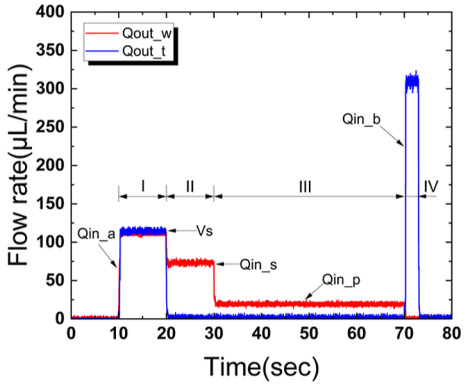

Figure 4. Measured flow rate of the working fluid for concentrating the target particles (Qin_a: flow rate of the microbead @ 40 kPa, Qin_p: flow rate of target of interest @ 20 kPa, Qin_b: flow rate of buffer @ 60 kPa, [I]: step I, fluid priming process, [II]: step II, trapping of microbeads, [III]: step III, target-binding process, and [IV]: step IV, elution process).

and target flow. Our measurements show that the flow rate was close to zero while the valve was closed. Thus, by leveraging the curved structure of the fluid chamber and flexibility of the PDMS diaphragm, an almost complete rubber seal valve is achieved.

2.2. Concentrating Microbeads in PDMFP-FAPCS. The particle enrichment presented in this paper is largely divided into two steps: streptavidin-coated bead enrichment and target enrichment. In the case of a centrifuge, it is determined that it is inappropriate to call it concentrated because only the density is different in the solution, and the fluid and beads + target are mixed. However, the fluid platform presented in this paper can discharge unnecessary fluid and greatly increase the concentration of beads + targets. In particular, it is judged to be more efficient for rare samples or small volumes. The platform presented here can be used to separate microbeads from targets without the need for washing.[50] There are several reasons a platform like the one presented here could be used to isolate microbeads. Unlike centrifuges, this platform allows selective and direct movement of microbeads. This makes it possible to achieve high-efficiency separations for biological analytes in biomedical applications.[51]

2.2.1. Step I to II: Concentration of Microbeads. Figure 5a–d illustrates the captured images showing the microbeads concentrated in the curved microchannel for 120 s when 10^6 ea/mL of beads were introduced into the microfluidic platform at a pressure of 40 kPa. A total of 4628 microbeads were accumulated at approximately 3.35×10^{-3} μL. On comparing the flow rate measured at the outlet port (Qout_w) when the flow is introduced (Qin_a), the concentration ratio was 992. No microbeads were observed when the 10 μL sample obtained from the outlet port (Qout_w) was analyzed using a disposable hemocytometer (INCYTO C-CipsTM). Thus, all the microbeads can be assumed to be trapped and accumulated successfully, as designed.

2.2.2. Step III: Conjugation. Figure 5e–i illustrates captured images showing the color change of microbeads coated with the GN6 aptamer, which exhibited high binding affinity and selectivity to Gram-negative bacterial strains,[52] while the EvaGreen-stained bacteria were introduced into the microchannel. The elapsed pretreatment process time for the target binding was 20 min. Images were captured every 5 min using a fluorescence microscope. Over time, the green color gradually darkened and expanded throughout the microchannel, and the *E. coli* bacteria bound well to the microbeads. Owing to the curved structure of the microchannel, a relatively large number of microbeads were concentrated at the center. Moreover, the flow rate at the central region of the microchannel was faster than that at the edge of the microchannel. Consequently, the color of the center with many microbeads and a high flow rate was stronger than that of the channel edge, which had a small number of microbeads. In other words, many targets can be captured in the middle region of the microchannel. When comparing the surface area of the 3D bead with that of the 2D channel, the surface area that can be captured by bacteria

Table 1. Fully Automated Pretreatment Process of Microbes Using the Microfluidic Platform

process	pneumatic input signal									fluidic output singal	
	reservoir			microvalve						flow rate (μL/min)	
	Qin_a	Qin_p	Qin_b	V_a	V_p	V_b	V_s	V_t	V_w	Qout_t	Qout_w
I	ON	OFF	OFF	OFF	ON	ON	OFF	OFF	OFF	Qin_a	Qin_a
II	ON	OFF	OFF	OFF	ON	ON	ON	ON	OFF	0	Qin_s
III	OFF	ON	OFF	ON	OFF	ON	ON	ON	OFF	0	Qin_p
IV	OFF	OFF	ON	ON	ON	OFF	OFF	OFF	ON	Qin_b	0

https://doi.org/10.1021/acsomega.3c02264
ACS Omega 2023, 8, 28344−28354

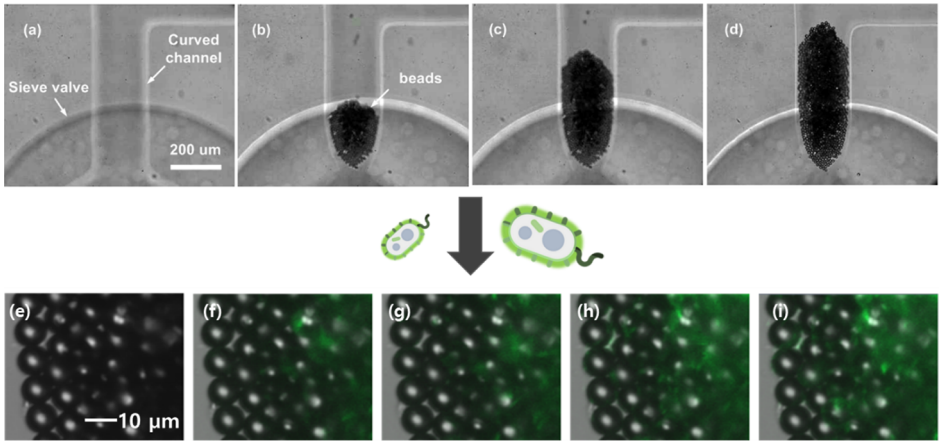

Figure 5. Concentrated microbeads in the microchannel before (a) and after (b–d) the concentration process of the microbeads. (a) before, (b) 40, (c) 80, and (d) 120 s. See Movie S1 for the performance of microbead capture on the curved fluid channel. Color change of the microbeads near the edge of the microfluidic channel was shown at (e) 0, (i) 5, (f) 10, (g) 15, and (h) 20 min.

Table 2. Targets and Specific Probing

Pollutant			Binding probe	Capturing target microbes/RBD-OMVs
bacteria	gram-negative bacteria	*Escherichia coli* (*E. coli*), DH5α	GN6 aptamer	
	gram-positive bacteria	*Streptococcus thermophilus*		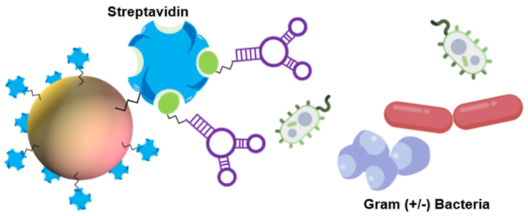
RBD-OMVs	SARS-CoV type 2 RBD displayed OMVs		Anti-SARS-CoV-2 RBD antibody	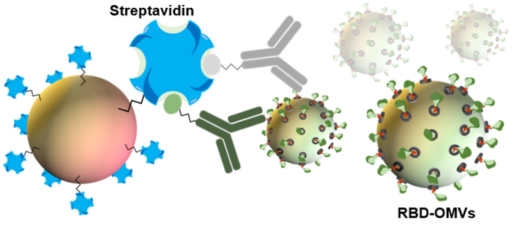

increases 42 times; therefore, the proposed method using the bead may be more efficient for the bacterial concentration.

2.2.3. Step IV: Selective and Quantitative Analysis of Particle Enrichment. Next, we sought to evaluate the selectivity and versatility of target enrichment in PDMFP-FAPCS. As a proof-of-concept study, a Gram-positive *Streptococcus thermophilus*, Gram-negative *E. coli*, and SARS-CoV-2 RBD-OMVs were selected as models (Table 2).

2.2.4. Selective Enrichment of Gram-Negative Bacteria. Figure 6a,b shows a graph of the number of Gram-negative and Gram-positive bacteria bound on the microbead-coated GN6 aptamers. Individual experiments were conducted to capture Gram-negative and Gram-positive bacteria using microbeads. After the elution of the microbeads in step IV, Qt was collected in sample tubes. For quantitative analysis, 100 microbeads were randomly obtained from the sample tube, dropped on a glass slide, and the number of EvaGreen-stained bacteria bound to the microbeads was observed and measured using a fluorescence microscope.

Figure 6a shows the number of Gram-negative bacteria bound to the microbeads. All but 16 beads had bacteria attached to them. Here, we hypothesized that the microbeads without bacteria attached to them were positioned near the edge of the curved microchannel. A total of 526 Gram-negative bacteria were attached to 82 beads. The number of beads with seven attached bacteria was highest at 18. As shown in Figure 6b, Gram-positive bacteria were attached to only two of the 100 beads, showing a significantly reduced binding efficiency.

In our study, bacterial 16s rDNA genes were amplified by a polymerase chain reaction (PCR). Genomic DNAs (gDNA) were isolated using the QIAamp DNA Mini Kit (Qiagen) following the manufacturer's protocol. Forward and reverse primer sets were tested for sensitivity, specificity, and priming efficiency as previously described.[53] The bacterial gDNA extracted from the concentrated microbead mixture was used as a template for PCR amplification. As is evident in Figure 6c, 16s rDNA of *E. coli* was amplified, and limit of detection (LOD) of *E. coli* was measured at 10^2 cfu/mL (Figure 6d).

https://doi.org/10.1021/acsomega.3c02264
ACS Omega 2023, 8, 28344−28354

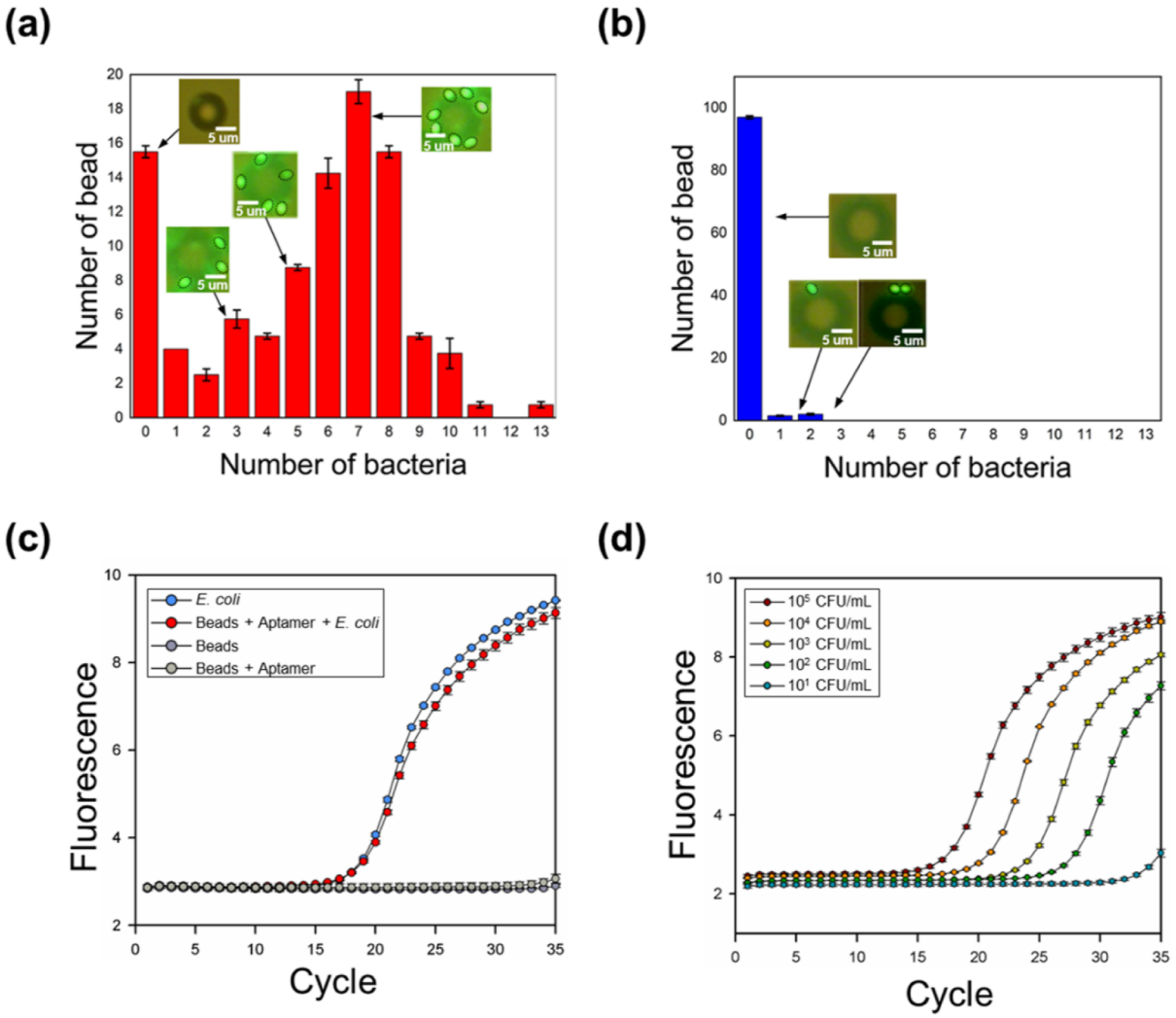

Figure 6. Number of bacteria bound to the aptamer-modified microbeads and bacterial DNA verification. (a) Gram-negative bacteria (n = 4), (b) Gram-positive bacteria (n = 4), and (c) amplification curves of the aptamer-microbead-bacteria isolates (red dot). Control 16s rDNA of *E. coli* were used as a positive control (blue dot), whereas beads and aptamer-modified microbeads were used as negative controls (deep gray and light gray dot, respectively). Each amplification curve is of three representative samples. (d) LOD of *E. coli* concentration (each n = 3). (ii) Nanovesicle enrichment: SARS-CoV-2 RBD-OMVs.

Drawing inspiration from the way that the SARS-CoV-2 S protein is highly conserved among all human coronaviruses and the RBD of the viral spike (S) protein helps the virus infect its host by latching on to the target cells, we reasoned that we could genetically engineer viral RBD to harbor into the bacterial cell membrane, followed by the formation of uniform spherical virus-mimetic OMVs. Bacterial antigen 43 (Ag43) comprises a signal peptide (1−52 aa), N-terminal unstructured passenger (53−137 aa), linker (138−600 aa), putative auto-chaperone (AC, 600−700 aa), and C-terminal β-barrel pore (701−1039 aa) (Figure S1a).[42,54] The β-barrel domain integrates into the bacterial outer membrane, where it forms a pore, and the passenger domain translocates through the β-barrel pore to the cell surface.[54] The plasmid named Ag43β-RBD inserts a passenger protein through genetic replacement of 53−137 aa (SARS-CoV-2 RBD). The entire bacterial expression of the Ag43β-RBD protein was examined by SDS−PAGE (Figure S1b). The Ag43β autotransporter expressing SARS-CoV-2 RBD prompted us to investigate more directly the outer membrane surface display of SARS-CoV-2 RBD.

The RBD-OMVs purified from the supernatant of cultured recombinant *E. coli* BL21 (DE3) cells are described in Figure 7a. We investigated the expression of RBD in combination with an autotransporter protein, Ag43, which forms an 18-stranded β-barrel on the outer membrane, and OmpF, outer membrane marker proteins (Figure 7a). In the dynamic light scattering analysis, the majority of the purified RBD-OMVs had a diameter of 150−300 nm. Also, they were observed to be in a spherical shape by cryo-transmission electron microscopy (cryo-TEM) (Figure 7b).

To confirm the enrichment of RBD-OMVs, RBD-OMVs were incubated with anti-SARS-CoV-2 Spike RBD-conjugated microbeads. Briefly, a biotinylated anti-SARS-CoV-2 Spike RBD antibody was conjugated to streptavidin-immobilized microbeads and mixed with OMVs derived from recombinant *E. coli* BL21 (DE3) cells. To examine whether RBD-OMVs could bind to the antibody-conjugated microbeads, 10^{12} particles of OMVs were introduced to microbeads in PDMFP-FAPCS. Subsequently, the recovered microbeads were investigated by scanning electron microscopy (SEM) (Figure 7c) and western blot analysis (Figure 7d). We observed that RBD-OMVs

https://doi.org/10.1021/acsomega.3c02264
ACS Omega 2023, 8, 28344−28354

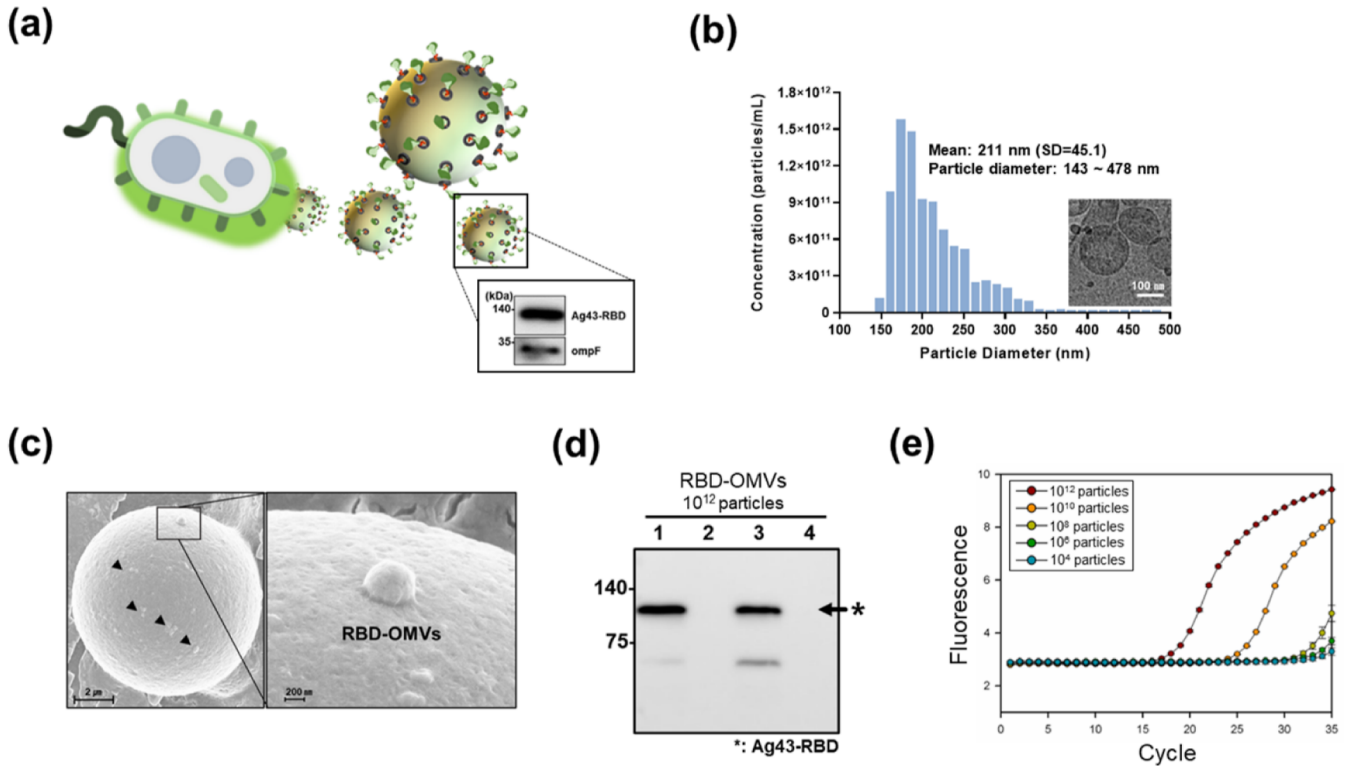

Figure 7. (a) Schematic images of RBD-OMVs from *E. coli* BL21(DE3) and the isolated OMVs were analyzed by western blotting using anti-SARS-CoV-2 Spike RBD antibody and anti-OmpF antibodies. (b) Size distribution of RBD-OMVs according to diameter as determined by dynamic light scattering and cryo-TEM image of purified RBD-OMVs. Scale bar, 100 nm. (c) Biotinylated anti-SARS-CoV-2 spike RBD antibody was conjugated to streptavidin- immobilized microbeads. PDMFP-FAPCS recovered RBD-OMVs were visualized under SEM [scale bar: 2 μm (left) and 200 nm(right)]. (d) Western blot analysis of recovered RBD-OMVs from FAPCS: FAPCS recovered microbeads (lane 1: beads and RBD-OMVs and lane 2: supernatant), after washing (lane 3: beads and RBD-OMVs and lane 4: supernatant). (e) LOD of RBD-OMVs using real-time PCR. Each experiment was measured three times.

attached to the antibody-conjugated microbeads were typically round in shape under SEM with a mean particle size of 211 nm. To confirm the LOD of RBD-OMVs through PDMFP-FAPCS, RT-PCR was applied as like an *E. coli* test and the LOD was 10^8 particles in this result (Figure 7e). These results indicate that PDMFP-FAPCS using antibody-immobilized affinity microbeads could be used to enrich intact nanovesicles, i.e., OMVs.

2.2.5. Comparison with Other Separation Technologies. The latest separation technologies compared with this study in Table 3 is an advancement of the previous technologies and have been developed with a focus on cost and performance improvement but lacks the most important automation and integration technology for portability and simplification. On the other hand, the simplified method has disadvantages of long operating time and high cost due to flow velocity limitation.[14,16,17,20−24,55−58]

The technology introduced in this study is a PDMFP that can concentrate and separate particles with only pneumatic pressure. It has high recovery efficiency and is reusable, requiring only initial cost. In addition, by using the FAPCS, which is easy to carry, we have built an automated system with improved performance, portability, and convenience. In the future, it is expected to evolve into a form with a built-in small-capacity compressor.

3. CONCLUSIONS

In this study, a disposable PDMFP using multiple pneumatic valves was proposed for microbead-based capture and enrichment of micro- and nano-sized pathogens. In addition, an FAPCS was developed to make the pretreatment process programmable. For example, performing individual injections of various fluids containing microbeads and targets over time and controlling pneumatic valves in the microfluidic platform. For this purpose, we tested PDMFP-FAPCS, which can enrich numerous specific targets with sizes ranging from micro- to nanoparticles. After optimizing the PDMFP-FAPCS operation, we explored the specific enrichment of target bacterial cells using an affinity probe, GN6 aptamer, and immobilized microbeads. Finally, we examined whether PDMFP-FAPCS could be applied to the enrichment of nanovesicles, i.e., OMVs. The specific antibody-immobilized microbeads have the potential to efficiently isolate a variety of nanovesicles. In conclusion, the results of this study demonstrate that the proposed PDMFP-FAPCS performs excellent enrichment of particles such as microbes and nanovesicles, which could be a promising tool for disease diagnosis and investigation as an effective pretreatment platform.

4. MATERIALS AND METHODS

4.1. Fabrication and Assembly. The interconnection layer is fabricated with a typical replica molding process. The valve diaphragm and bottom layer are prepared using the spin-coating and the curing process of liquid PDMS. As a core structure of the microfluidic platform, the double-sided replication process with two SU-8 molds is employed to fabricate the 3D fluidic network with the curved pneumatic valve chambers and microfluidic

https://doi.org/10.1021/acsomega.3c02264
ACS Omega 2023, 8, 28344−28354

Table 3. Comparison to Other Separation Techniques with This Platform

microfluidic method	sample	sample flow rate	separation time	concentration rate	separation efficiency	recovery efficiency	additional equipment	recycle and cost	refs
magnetophoretic	3.2, and 4.8 μm beads	<6 μL/min	N.A	N.A	76%		pressure controller, NdFeB magnets	possible (high cost due to the use of magnetic particles)	14
electrokinetic	MDA-MB-231 and HeLa cells	0.1 μL/min	N.A	N.A	98%	98% (cancer cells)	syringe pump, function generator	possible (high cost due to the use of magnetic particles)	16
acoustophoresis	*Pseudomonas aeruginosa* and blood cells	400 μL/min	12.5 min	N.A	99%	90% (bacteria)	pressure terminal, PID regulator	Possible (low cost)	17
sedimentation	human blood	10−30 μL/min	N.A	N.A	99%	66% (plasma)	syringe pump, glass tube	impossible (chip production cost)	20
hydrodynamic filtration	1−3 μm beads	1 μL/min	60 min	2000−5000%	80%	60% (beads)	syringe pump	impossible (chip production cost)	21
pinched flow fractionation	3.0 and 5.0 μm beads	2060 μL/h	5 min	N.A	93.7%	93.7% (beads)	spinning device	possible (low processing speed)	22
lateral displacement	2.1, 4.2, and 5.7 μm beads	0.59 μL/min	20 min	N.A	96%	99% (beads)	syringe pump	possible (low processing speed)	23
inertial effects	3/10 μm and 5/13 μm beads	600 μL/min	N.A	99% (beads, human blood cells, and erythroleukemia cells)	>99%	>99% (beads, human blood cells, and erythroleukemia cells)	syringe pump	possible (high cost due to the use of magnetic particles)	24
microsphere stacking, plasma separation	10, 20, 100 μm beads, venous blood	600 μL/min	55 min	protein (TP): 21.203 ± 2.205 g/L, albumin (ALB): 4.978 ± 0.765 g/L, glucose (GLU): 0.043 ± 0.012 g/L, and uric acid (UA): 0.005 ± 0.001 g/L (increase compared to centrifugal sample)	11%	11% (plasma)	syringe pump	impossible (chip production cost)	55
electrokinetics deterministic lateral displacement (eDLD)	*E. coli* and *Saccharomyces cerevisiae*	0.86−0.92 μL/h	1 h 30 min	60−70 g/L	86%	86% (bacteria)	pressure controller, function generator	impossible (chip production cost)	56
viscoelastic focusing separation	cell culture supernatant and serum	200 μL/h	1 h	N/A	90% (EVs)	80% (EVs)	syringe pump	impossible (chip production cost)	57
sequential surface acoustic wave	blood	4 μL/min	25 min	N/A	98.4% (EVs)	82.4% (EVs)	syringe pumps, cooling system, function generator	impossible (low processing speed)	58
pneumatically driven microfluidic platform (PDMFP)	10 μm beads (bead size no matter)	112.926 μL/min	20 min	99,200% (beads)	100% (beads)	100% (beads)	FAPCS	possible (detecting particle cost only)	this study

https://doi.org/10.1021/acsomega.3c02264
ACS Omega 2023, 8, 28344−28354

channels at the front and interconnection channels at the back.[44] The prepared PDMS layers are sequentially bonded using corona discharge treatment.

4.2. Bacterial Strains and Media. Glycerol stocks of *E. coli* DH5α (Invitrogen, Carlsbad, CA) strain and *S. thermophilus* (ATCC 19258) were streaked onto LB solid medium (10 g L^{-1} Bacto tryptone, 5 g L^{-1} Bacto yeast extract, 10 g L^{-1} NaCl, and 15 g L^{-1} agar) and cultured at 30 °C. A single colony was then inoculated into 3 mL of LB medium and cultured at 30 °C with constant shaking overnight. The culture was diluted into 1:100 in fresh LB media and then cultured at 30 °C to the mid-exponential phase (optical density, OD_{600} = 0.6).

4.3. Fluorescent Staining and Enrichment of Bacteria. *E. coli* DH5α (3×10^5 cfu/mL) was mixed with 5 μL of EvaGreen (Biotium Inc., Hayward, CA, USA) and 365 μL of deionized water, followed by incubation in the dark for 15 min. Bacterial green fluorescence signals were measured using a fluorescence microscope (Olympus IX-81, Japan). For the bacterial enrichment, 5 μg of streptavidin-coated polystyrene microbeads (Spherotech, SVP-100-4, Illinois, USA) ($\sim 2.0 \times 10^8$ beads) was incubated overnight at 4 °C with 2 μg of biotinylated GN6 aptamer in 50 μL of PBS and then aptamer-modified microbeads were stored for up to 2 weeks at 4 °C.

4.4. Bacterial Genomic DNA Extraction and Gene Amplification Analysis. A single colony of *E. coli* DH5α strain was suspended in 20 μL of sterile water. Genomic DNA (gDNA) was isolated using the QIAamp DNA Mini Kit (Qiagen) following the manufacturer's protocol. Forward and reverse primer sets were tested for sensitivity, specificity, and priming efficiency as previously described.[59] Real-time PCR was performed using a Mic qPCR Cycler (Bio Molecular Systems, Australia). The PCR reaction mixture contains 10 μL of 2× SYBR Master Mix (Bio-rad), 10 pmol forward and reverse primers, and 1 μL of template gDNA. Following the PCR, water was added to obtain a final reaction volume of 20 μL. The amplification conditions for the multiplex assay were set as follows: pre-denaturation at 95 °C for 3 min, followed by 35 cycles of denaturation at 95 °C for 10 s, and annealing/extension at 55 °C for 30 s.

4.5. Expression of Ag43-Integrated RBD Protein and Outer Membrane Purification. *E. coli* BL21 (DE3) cells transformed with pET-28b-Ag43β-RBD were grown in LB liquid medium at 37 °C for overnight at 200 rpm. Protein expression was induced with 0.5 and 1 mM isopropyl β-D-1-thiogalactopyranoside (IPTG) at 25 °C for 20 h at 200 rpm. Cells were harvested at 5000*g* for 20 min, washed once with 200 mM Tris-HCl (pH = 8.0) and then further centrifuged. The pellet was resuspended in a solution containing 200 mM Tris-HCl. The isolation of OMVs was performed as a previously reported method with slight modification.[60] The purified OMVs were dispersed in DPBS buffer (Welgene, Gyeongsan, Republic of Korea) and stored to −80 °C, until further use.

4.6. RBD-OMV Characterization. The size and concentration of OMVs were determined using the qNano Gold instrument (Izon, Australia). For cryo-EM, a carbon-coated Cu mesh grid (electron microscopy science) was used. Images were collected at a magnification of 14,500× up to 25,000× on a Tecnai G2 F20 TWIN TMP operating at 200 kV. For western blot, the SARS-CoV-2 spike protein RBD monoclonal antibody (OriGene, USA) and polyclonal anti-OmpF (Abcam, UK) were used in this study. Antibody-attached PVDF membrane was further developed using WesternBright ECL (Advansta, USA) and immediately imaged using Amersham Imager 600 (GE Healthcare, USA).

4.7. Microbead-RBD-OMV Binding. For biotinylated RBD antibody (biotin-RBD Ab), a biotinylation kit was used according to the kit manual (Abcam, UK). Microbeads and biotin-RBD Ab were incubated to 24 h at 4 °C with rotation and centrifuged at 15,000*g* for 5 min at 4 °C to remove unbounded antibody. After concentration, these were further used on SEM, immunoblotting, and real-time PCR.

4.8. Scanning Electron Microscopy. The samples were fixed with 2.5% glutaraldehyde/4% paraformaldehyde and incubated O/N at 4 °C. Finally, the samples were dehydrated by passing them through a graded series of ethanol concentrations (up to 100%). The morphology was then observed using a field emission scanning electron microscope (ULTRA PLUS, Carl Zeiss, Germany).

4.9. Immunoblotting and Real-Time PCR to Confirm Microbead-Conjugated RBD-OMVs. 20 μL of microbead and RBD-OMV binding complex were loaded into 10% SDS−PAGE gel and transferred to the PVDF membrane. Immunoblotting procedure was the same procedure as mentioned above for RBD-OMV characterization. Real-time PCR was the same procedure as mentioned above for bacterial genomic DNA extraction and gene amplification analysis.

■ ASSOCIATED CONTENT

Supporting Information

The Supporting Information is available free of charge at https://pubs.acs.org/doi/10.1021/acsomega.3c02264.

Design of outer membrane-targeted Ag43β-RBD and operating FAPCS (PDF)

Performance of microbead capture on the curved fluid channel (MP4)

■ AUTHOR INFORMATION

Corresponding Authors

Ji-Young Ahn − *Center for Ecology and Environmental Toxicology, Chungbuk National University, Cheongju 28644, Republic of Korea; Department of Microbiology, Chungbuk National University, Cheongju 28644, Republic of Korea;* orcid.org/0000-0002-3729-2284; Email: jyahn@chungbuk.ac.kr

Ok Chan Jeong − *Department of Digital Anti-Aging Health Care, Inje University - Gimhae Campus, Gimhae 50834, Republic of Korea; Department of Biomedical Engineering, Inje University - Gimhae Campus, Gimhae 50834, Republic of Korea*; Email: memsoku@inje.ac.kr

Authors

Hong Jin Choi − *Department of Digital Anti-Aging Health Care, Inje University - Gimhae Campus, Gimhae 50834, Republic of Korea;* orcid.org/0000-0001-9170-2670

Gna Ahn − *Center for Ecology and Environmental Toxicology, Chungbuk National University, Cheongju 28644, Republic of Korea*

U Seok Yu − *Department of Biomedical Engineering, Inje University - Gimhae Campus, Gimhae 50834, Republic of Korea*

Eun Jin Kim − *Department of Digital Anti-Aging Health Care, Inje University - Gimhae Campus, Gimhae 50834, Republic of Korea*

Complete contact information is available at:

https://pubs.acs.org/10.1021/acsomega.3c02264

Author Contributions

Conceptualization, O.C.J. and J-Y.A.; methodology, O.C.J. and J-Y.A.; software, H.J.C., U.S.Y., and E.J.K.; formal analysis, H.J.C. and J-Y.A.; investigation, G.A., H.J.C., and E.J.K.; data curation, O.C.J. and J-Y.A.; writing—original draft preparation, O.C.J. and J-Y.A.; and writing—review and editing, O.C.J. and J-Y.A. All authors have read and agreed to the published version of the manuscript.

Notes

The authors declare no competing financial interest.

■ ACKNOWLEDGMENTS

This work was supported by the National Research Foundation of Korea (NRF) grant funded by the Korea government (Ministry of Science and ICT) (2021R1A2C1011380). This work was also supported by a Basic Science Research Program through the National Research Foundation of Korea (NRF) funded by the Ministry of Education (2020R1A6A1A06046235) and Chungbuk National University in 2022.

■ REFERENCES

(1) Cheng, Y.; Ye, X.; Ma, Z.; Xie, S.; Wang, W. High-throughput and clogging-free microfluidic filtration platform for on-chip cell separation from undiluted whole blood. *Biomicrofluidics* **2016**, *10*, 014118.
(2) Zhang, S. Z.; Wang, Y.; Onck, P.; den Toonder, J. A concise review of microfluidic particle manipulation methods. *Microfluid. Nanofluid.* **2020**, *24*, 24.
(3) Jackson, E. L.; Lu, H. Advances in microfluidic cell separation and manipulation. *Curr. Opin. Chem. Eng.* **2013**, *2*, 398−404.
(4) Li, P.; Mao, Z. M.; Peng, Z. L.; Zhou, L. L.; Chen, Y. C.; Huang, P. H.; Truica, C. I.; Drabick, J. J.; El-Deiry, W. S.; Dao, M.; Suresh, S.; Huang, T. J. Acoustic separation of circulating tumor cells. *Proc. Natl. Acad. Sci. U.S.A.* **2015**, *112*, 4970−4975.
(5) Sun, C.; Hsieh, Y. P.; Ma, S.; Geng, S.; Cao, Z.; Li, L.; Lu, C. Immunomagnetic separation of tumor initiating cells by screening two surface markers. *Sci. Rep.* **2017**, *7*, 40632.
(6) Huang, W.; Chang, C. L.; Brault, N. D.; Gur, O.; Wang, Z.; Jalal, S. I.; Low, P. S.; Ratliff, T. L.; Pili, R.; Savran, C. A. Separation and dual detection of prostate cancer cells and protein biomarkers using a microchip device. *Lab Chip* **2017**, *17*, 415−428.
(7) Lee, W.; Tseng, P.; Carlo, D. D. *Microtechnology for Cell Manipulation and Sorting*; Springer: Cham, 2017.
(8) Jiang, D.; Liu, S.; Tang, W. Fabrication and Manipulation of Non-Spherical Particles in Microfluidic Channels: A Review. *Micromachines* **2022**, *13*, 1659.
(9) Xue, L. J.; Jiang, F.; Xi, X.; Li, Y.; Lin, J. Lab-on-chip separation and biosensing of pathogens in agri-food. *Trends Food Sci. Technol.* **2023**, *137*, 92−103.
(10) Zhang, X.; Xu, X.; Wang, J.; Wang, C.; Yan, Y.; Wu, A.; Ren, Y. Public-Health-Driven Microfluidic Technologies: From Separation to Detection. *Micromachines* **2021**, *12*, 391.
(11) Bunyakul, N.; Baeumner, A. J. Combining electrochemical sensors with miniaturized sample preparation for rapid detection in clinical samples. *Sensors* **2015**, *15*, 547−564.
(12) Dalili, A.; Samiei, E.; Hoorfar, M. A review of sorting, separation and isolation of cells and microbeads for biomedical applications: microfluidic approaches. *Analyst* **2019**, *144*, 87−113.
(13) Sajeesh, P.; Sen, A. K. Particle separation and sorting in microfluidic devices: a review. *Microfluid. Nanofluid.* **2014**, *17*, 1−52.
(14) Munaz, A.; Shiddiky, M. J. A.; Nguyen, N. T. Magnetophoretic separation of diamagnetic particles through parallel ferrofluid streams. *Sens. Actuators B Chem.* **2018**, *275*, 459−469.
(15) Modarres, P.; Tabrizian, M. Frequency hopping dielectrophoresis as a new approach for microscale particle and cell enrichment. *Sens. Actuators B Chem.* **2019**, *286*, 493−500.
(16) Gao, J.; Riahi, R.; Sin, M. L.; Zhang, S.; Wong, P. K. Electrokinetic focusing and separation of mammalian cells in conductive biological fluids. *Analyst* **2012**, *137*, 5215−5221.
(17) Friend, J.; Yeo, L. Y. Microscale acoustofluidics: Microfluidics driven via acoustics and ultrasonics. *Rev. Mod. Phys.* **2011**, *83*, 647−704.
(18) Shen, Y. G.; Yalikun, Y.; Tanaka, Y. Recent advances in microfluidic cell sorting systems. *Sens. Actuators B Chem.* **2019**, *282*, 268−281.
(19) Mach, A. J.; Kim, J. H.; Arshi, A.; Hur, S. C.; Di Carlo, D. Automated cellular sample preparation using a Centrifuge-on-a-Chip. *Lab Chip* **2011**, *11*, 2827−2834.
(20) Zhang, X. B.; Wu, Z. Q.; Wang, K.; Zhu, J.; Xu, J. J.; Xia, X. H.; Chen, H. Y. Gravitational sedimentation induced blood delamination for continuous plasma separation on a microfluidics chip. *Anal. Chem.* **2012**, *84*, 3780−3786.
(21) Yamada, M.; Seki, M. Hydrodynamic filtration for on-chip particle concentration and classification utilizing microfluidics. *Lab Chip* **2005**, *5*, 1233−1239.
(22) Morijiri, T.; Sunahiro, S.; Senaha, M.; Yamada, M.; Seki, M. Sedimentation pinched-flow fractionation for size- and density-based particle sorting in microchannels. *Microfluid. Nanofluid.* **2011**, *11*, 105−110.
(23) Hochstetter, A.; Vernekar, R.; Austin, R. H.; Becker, H.; Beech, J. P.; Fedosov, D. A.; Gompper, G.; Kim, S. C.; Smith, J. T.; Stolovitzky, G.; Tegenfeldt, J. O.; Wunsch, B. H.; Zeming, K. K.; Kruger, T.; Inglis, D. W. Deterministic Lateral Displacement: Challenges and Perspectives. *ACS Nano* **2020**, *14*, 10784−10795.
(24) Zhang, J.; Yan, S.; Sluyter, R.; Li, W.; Alici, G.; Nguyen, N. T. Inertial particle separation by differential equilibrium positions in a symmetrical serpentine micro-channel. *Sci. Rep.* **2014**, *4*, 4527.
(25) Shen, S.; Zhang, F.; Wang, S.; Wang, J.; Long, D; Wang, D.; Niu, Y. Ultra-low aspect ratio spiral microchannel with ordered micro-bars for flow-rate insensitive blood plasma extraction. *Sens. Actuators B Chem.* **2019**, *287*, 320−328.
(26) Du, G.; Fang, Q.; den Toonder, J. M. J. Microfluidics for cell-based high throughput screening platforms - A review. *Anal. Chim. Acta* **2016**, *903*, 36−50.
(27) Yeo, L. Y.; Chang, H. C.; Chan, P. P. Y.; Friend, J. R. Microfluidic devices for bioapplications. *Small* **2011**, *7*, 12−48.
(28) Zhang, C.; Xing, D. Single-molecule DNA amplification and analysis using microfluidics. *Chem. Rev.* **2010**, *110*, 4910−4947.
(29) Chen, X. Y.; Shen, J. N. Review of membranes in microfluidics. *J. Chem. Technol. Biotechnol.* **2017**, *92*, 271−282.
(30) Han, S. J.; Park, H. K.; Kim, K. S. Applications of Microfluidic Devices for Urology. *Int. Neurourol. J.* **2017**, *21*, S4−S9.
(31) McNerney, R.; Daley, P. Towards a point-of-care test for active tuberculosis: obstacles and opportunities. *Nat. Rev. Microbiol.* **2011**, *9*, 204−213.
(32) Mancera-Andrade, E. I.; Parsaeimehr, A.; Arevalo-Gallegos, A.; Ascencio-Favela, G.; Parra Saldivar, R. Microfluidics technology for drug delivery: A review. *Front. Biosci.* **2018**, *10*, 74−91.
(33) Li, B.; Li, L.; Guan, A.; Dong, Q.; Ruan, K.; Hu, R.; Li, Z. A smartphone controlled handheld microfluidic liquid handling system. *Lab Chip* **2014**, *14*, 4085−4092.
(34) Watson, C.; Senyo, S. All-in-one automated microfluidics control system. *HardwareX* **2019**, *5*, e00063.
(35) Zhang, Y.; Tseng, T. M.; Schlichtmann, U. Portable all-in-one automated microfluidic system (PAMICON) with 3D-printed chip using novel fluid control mechanism. *Sci. Rep.* **2021**, *11*, 19189.
(36) Zhao, X.; Li, M.; Liu, Y. Microfluidic-Based Approaches for Foodborne Pathogen Detection. *Microorganisms* **2019**, *7*, 381.
(37) Tiku, V.; Tan, M. W. Host immunity and cellular responses to bacterial outer membrane vesicles. *Trends Immunol.* **2021**, *42*, 1024−1036.
(38) Xia, B.; Pan, X.; Luo, R. H.; Shen, X.; Li, S.; Wang, Y.; Zuo, X.; Wu, Y.; Guo, Y.; Xiao, G.; Li, Q.; Long, X. Y.; He, X. Y.; Zheng, H. Y.;

Lu, Y.; Pang, W.; Zheng, Y. T.; Li, J.; Zhang, L. K.; Gao, Z. Extracellular vesicles mediate antibody-resistant transmission of SARS-CoV-2. *Cell Discovery* **2023**, *9*, 2.
(39) Ahn, G.; Lee, S. H.; Song, M. S.; Han, B. K.; Kim, Y. H.; Ahn, J. Y. JEV-nanobarcode and colorimetric reverse transcription loop-mediated isothermal amplification (cRT-LAMP). *Mikrochim. Acta* **2021**, *188*, 333.
(40) Kaper, J. B.; Nataro, J. P.; Mobley, H. L. Pathogenic Escherichia coli. *Nat. Rev. Microbiol.* **2004**, *2*, 123−140.
(41) Sekhon, S. S.; Shin, W. R.; Kim, S. Y.; Jeong, D. S.; Choi, W.; Choi, B. K.; Min, J.; Ahn, J. Y.; Kim, Y. H. Cyclophilin A-mediated mitigation of coronavirus SARS-CoV-2. *Bioeng. Transl. Med.* **2022**, *8*, e10436.
(42) Jing, K. J.; Guo, Y.; Ng, I. S. Antigen-43-mediated surface display revealed in Escherichia coli by different fusion sites and proteins. *Bioresour. Bioprocess.* **2019**, *6*, 14.
(43) Metruccio, M. M. E.; Evans, D. J.; Gabriel, M. M.; Kadurugamuwa, J.; Fleiszig, S. M. J. Outer Membrane Vesicle shedding by P. aeruginosa is Induced by Tear Fluid or Lysozyme and Compromises Corneal Epithelial Defenses Against Bacterial Adhesion and Traversal. *Invest. Ophthalmol. Visual Sci.* **2014**, *55*, 6254.
(44) Jang, J. H.; Jeong, O. C. Fabrication of a Pneumatic Microparticle Concentrator. *Micromachines* **2020**, *11*, 40.
(45) Oh, C. K.; Lee, S. W.; Jeong, O. C. Fabrication of pneumatic valves with spherical dome-shape fluid chambers. *Microfluid. Nanofluid.* **2015**, *19*, 1091−1099.
(46) Wu, W.; Wu, J.; Kim, J. H.; Lee, N. Y. Instantaneous room temperature bonding of a wide range of non-silicon substrates with poly(dimethylsiloxane) (PDMS) elastomer mediated by a mercapto-silane. *Lab Chip* **2015**, *15*, 2819−2825.
(47) Nikcevic, I.; Bange, A.; Peterson, E. T.; Papautsky, I.; Heineman, W. R.; Halsall, H. B.; Seliskar, C. J. Adsorption of fluorescently labeled microbeads on PDMS surfaces. *Proc. SPIE 5718, Microfluidics, BioMEMS, and Medical Microsystems III* **2005**, *5718*, 159−167.
(48) Burger, R.; Reith, P.; Kijanka, G.; Akujobi, V.; Abgrall, P.; Ducrée, J. Array-based capture, distribution, counting and multiplexed assaying of beads on a centrifugal microfluidic platform. *Lab Chip* **2012**, *12*, 1289−1295.
(49) Straub, H.; Bigger, C. M.; Valentin, J.; Abt, D.; Qin, X. H.; Eberl, L.; Maniura-Weber, K.; Ren, Q. Bacterial adhesion on soft materials: passive physicochemical interactions or active bacterial mechanosensing? *Adv. Healthcare Mater.* **2019**, *8*, 1801323.
(50) Wang, J.; Ma, J.; Wen, X. Basic Concepts of Density Gradient Ultracentrifugation. *Nanoseparation Using Density Gradient Ultracentrifugation: Mechanism. Methods and Applications*; Springer, 2018; pp 21−36.
(51) Sajjad, U.; Klingbeil, F.; Block, F.; Hollander, R. B.; Bhatti, S.; Lage, E.; McCord, J. Efficient flowless separation of mixed microbead populations on periodic ferromagnetic surface structures. *Lab Chip* **2021**, *21*, 3174−3183.
(52) Shin, H. S.; Gedi, V.; Kim, J. K.; Lee, D. K. Detection of Gram-negative bacterial outer membrane vesicles using DNA aptamers. *Sci. Rep.* **2019**, *9*, 13167.
(53) Aggarwal, D.; Kanitkar, T.; Narouz, M.; Azadian, B. S.; Moore, L. S. P.; Mughal, N. Clinical utility and cost-effectiveness of bacterial 16S rRNA and targeted PCR based diagnostic testing in a UK microbiology laboratory network. *Sci. Rep.* **2020**, *10*, 7965.
(54) Ageorges, V.; Schiavone, M.; Jubelin, G.; Caccia, N.; Ruiz, P.; Chafsey, I.; Bailly, X.; Dague, E.; Leroy, S.; Paxman, J.; Heras, B.; Chaucheyras-Durand, F.; Rossiter, A. E.; Henderson, I. R.; Desvaux, M. Differential homotypic and heterotypic interactions of antigen 43 (Ag43) variants in autotransporter-mediated bacterial autoaggregation. *Sci. Rep.* **2019**, *9*, 11100.
(55) Xu, H.; Wu, Z.; Deng, J.; Qiu, J.; Hu, N.; Gao, L.; Yang, J. Microsphere-Based Microfluidic Device for Plasma Separation and Potential Biochemistry Analysis Applications. *Micromachines* **2021**, *12*, 487.
(56) Ho, B. D.; Beech, J. P.; Tegenfeldt, J. O. Cell Sorting Using Electrokinetic Deterministic Lateral Displacement. *Micromachines* **2021**, *12*, 30.
(57) Zhou, Y.; Ma, Z.; Tayebi, M.; Ai, Y. Submicron Particle Focusing and Exosome Sorting by Wavy Microchannel Structures within Viscoelastic Fluids. *Anal. Chem.* **2019**, *91*, 4577−4584.
(58) Wu, M.; Ouyang, Y.; Wang, Z.; Zhang, R.; Huang, P. H.; Chen, C.; Li, H.; Li, P.; Quinn, D.; Dao, M.; Suresh, S.; Sadovsky, Y.; Huang, T. J. Isolation of exosomes from whole blood by integrating acoustics and microfluidics. *Proc. Natl. Acad. Sci. U.S.A.* **2017**, *114*, 10584−10589.
(59) Weisburg, W. G.; Barns, S. M.; Pelletier, D. A.; Lane, D. J. 16S ribosomal DNA amplification for phylogenetic study. *J. Bacteriol.* **1991**, *173*, 697−703.
(60) Park, M.; Yoo, G.; Bong, J. H.; Jose, J.; Kang, M. J.; Pyun, J. C. Isolation and characterization of the outer membrane of Escherichia coli with autodisplayed Z-domains. *Biochim. Biophys. Acta, Biomembr.* **2015**, *1848*, 842−847.

https://doi.org/10.1021/acsomega.3c02264
ACS Omega 2023, 8, 28344−28354